Inclined Links Hyper-Redundant Elephant Trunk-Like Robot

Oded Salomon, Alon Wolf
Biorobotics and Biomechanics Lab
Faculty of Mechanical Engineering, Technion-I.I.T.
Haifa 32000, Israel
Tel: 972-4-8292087, Fax: 972-4-8295711, Email: odeds/alonw@technion.ac.il

Abstract

Hyper-redundant robots (HRR) have many more degrees of freedom (DOF) than required, which enable them to handle more constraints, such as those present in highly convoluted volumes. Consequently, they can serve in many robotic applications, while extending the reachability and manoeuvrability of the operator. The many degrees of freedom that furnish the HRR with its wide range of capabilities also provide its major challenges: mechanism design, control, and path planning. In this paper, we present a novel design of a HRR composed of sixteen DOF. The HRR is composed of two concentric structures: a passive backbone and an exoskeleton which carries self-weight as well as external loads. The HRR is 80 cm long, 7.7 cm in diameter, achieves high rigidity and accuracy and is capable of 180° bending. The forward kinematics of the HRR is presented along with the inverse kinematics of a link.

Keywords: hyper-redundant arm, robot manipulator, snake robot

1. Introduction

A redundant robot has at least one more degree of freedom (DOF) than required, in order to compensate for simple constraints, i.e., using an elbow up versus an elbow down configuration, to reach a target position. Hyper-redundant robots (HRR) have many more DOF than required, which enable them to handle more constraints, such as those present in highly convoluted volumes, and at the same time enable them to perform a variety of tasks. It is no surprise that HRR are versatile - look at their biological counterparts: snakes, elephant trunks, and worms, all of which can poke through and crawl through crevices as well as manipulate objects. Starting in 1972 with Hirose's [1] pioneering work in HRR design, following with the work of Chirikjian and Burdick [2], there has been considerable attention paid to HRR design. The manoeuvrability inherent in these types of mechanical structures and their compliance, i.e., their ability to conform to environmental constraints, allow them to overcome obstacles of significant complexity compared to conventional robots, hence they have become a challenge for robotic mechanism designers [3, 4]. Recently, other researchers, such as Yim [5] at PARC, Miller [6, 7] on his own, and Haith at NASA Ames [8], have extended Hirose's pioneering work on snake locomotion, where Yim and Haith used Yim's Polybot modules to design a modular hyper-redundant robot. Takanashi developed at NEC [9, 10] a new two-DOF joint for snake robots that allowed a more compact design. This joint used a passive universal joint to prevent adjacent bays from twisting while at the same time allowing two degrees of freedom: bending and orienting. This universal joint was enveloped an angular swivel joint, which provided the two degrees of freedom. The universal joint, which was installed on the outside, rendered the joint relatively bulky. Researchers at the JPL [11] "inverted" Takanashi's design by placing a small universal joint in the interior of the robot. This allowed for a more compact design, but came at the cost of strength and stiffness (backlash). Other known designs use cable/tendon actuation systems for driving the robot, yet these designs are somewhat cumbersome and require quite a large external driving system [1, 3, 12]. Ma et. al have also presented the mechanical design of a HRR and its control algorithm for the inspection of confined spaces [13]. An actuated universal-joint design was presented in [14]. For this design, U-joint "crosses" are connected to one link with a pitch pivot joint, and

to the next with a yaw pivot joint. The pitch and yaw joints are always orthogonal, and intersect along the link centrelines; this leads to a relatively simple kinematic system. The pitch and yaw joints are actuated by linear actuators placed within the link's envelope. The links are configured such that the axes at each end of any link are parallel; thus, one link has pitch joints at both ends actuated by its two linear actuators; the next link has two yaw joints. This arrangement facilitates packaging of the two linear actuators side-by-side within the link. In [15], the authors reported on design of a new lightweight, hyper-redundant, deployable Binary Robotic Articulated Intelligent Device (BRAID), for space robotic systems. The BRAID is intended to meet the challenges of future space robotic systems that need to perform more complex tasks than are currently feasible. It is lightweight, has a high degree of freedom, and has a large workspace. The device is based on embedded muscle type binary actuators and flexure linkages. Such a system may be used for a wide range of tasks, and requires minimal control computation and power resources. In [16], the authors used wires to design a wire-driven weight-compensation mechanism. The mechanism consisted of a parallelogram linkage mechanism that had an extended portion with the wired double pulley.

In the current report, we present a novel design composed of sixteen degrees of freedom (DOF) using serially chained links (Figure 1a). The hyper-redundant arm was designed to maximise precision and strength. These goals were achieved by constructing an arm composed of two concentric skeletons: internal and external. The internal skeleton is responsible for the kinematics of the arm and serves as a backbone, whereas the external skeleton serves as a mechanical "exoskeleton" carrying the self-weight of the arm and the external loads. Total length of the arm is 80 cm, curving to an overall bend of up to 180° and capable of manipulating its own weight with an additional payload of 25% at its tip (at horizontal stretch) which can be equipped with a camera or a gripper.

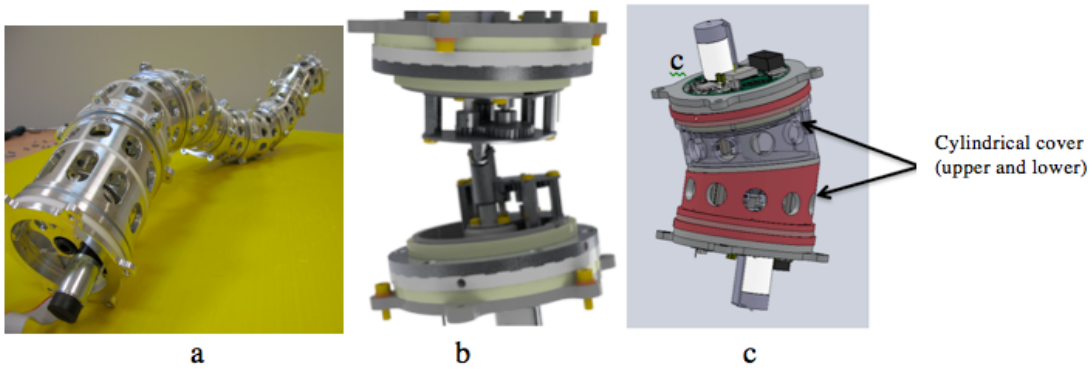

Figure 1: a) Full model of the 16DOF arm b) a single link universal joint backbone c) Cylindrical cover

2. Mechanical Architecture of the Mechanism and low level controller

2.1 Mechanical architecture

The HRR arm is composed of eight modular links (Figure 1a). The links are connected by centralised passive universal joints (Figure 1b) surrounded by a cylindrical cover (Figure 1c). The cylindrical cover is decomposed into two cylinders, upper and lower, connected along two 11.25° inclined planes, facing opposite each other (Figure 2a). The two cylinders can be rotated independently using two axially positioned DC motors through a 22:1 external gear (Figures 3 and 4). Relative rotation of the motors results in an inclination angle of 0-22.5° between the centrelines of the upper and lower cylinders (Figure 2b). When both motors are rotated simultaneously in the same direction and speed, the inclined link rotates 360° around the link's vertical axis (Figure 2b). Consequently, the orientation of the inclination of that link is rotated 0-360° in free space.

One of the biggest challenges in the design of a hyper-redundant long manipulator is maintaining reasonable dimensions and low self-weight, while not compromising the rigidity of the structure and its accuracy. Usually, these design criteria are counter-intuitive, i.e. rigidity is usually achieved by large physical dimensions and high self-weight. The novelty of the proposed structure is that it achieves high rigidity and accuracy while still maintaining a relatively low weight of 480 g per link at a total length of 800 mm and an outer diameter of 77 mm.

As described before, the inclination angle of the link is achieved by rotating one the cylinder with respect to another. Also, the orientation of the inclined cylinder is achieved by a synchronised rotation of both cylinders.

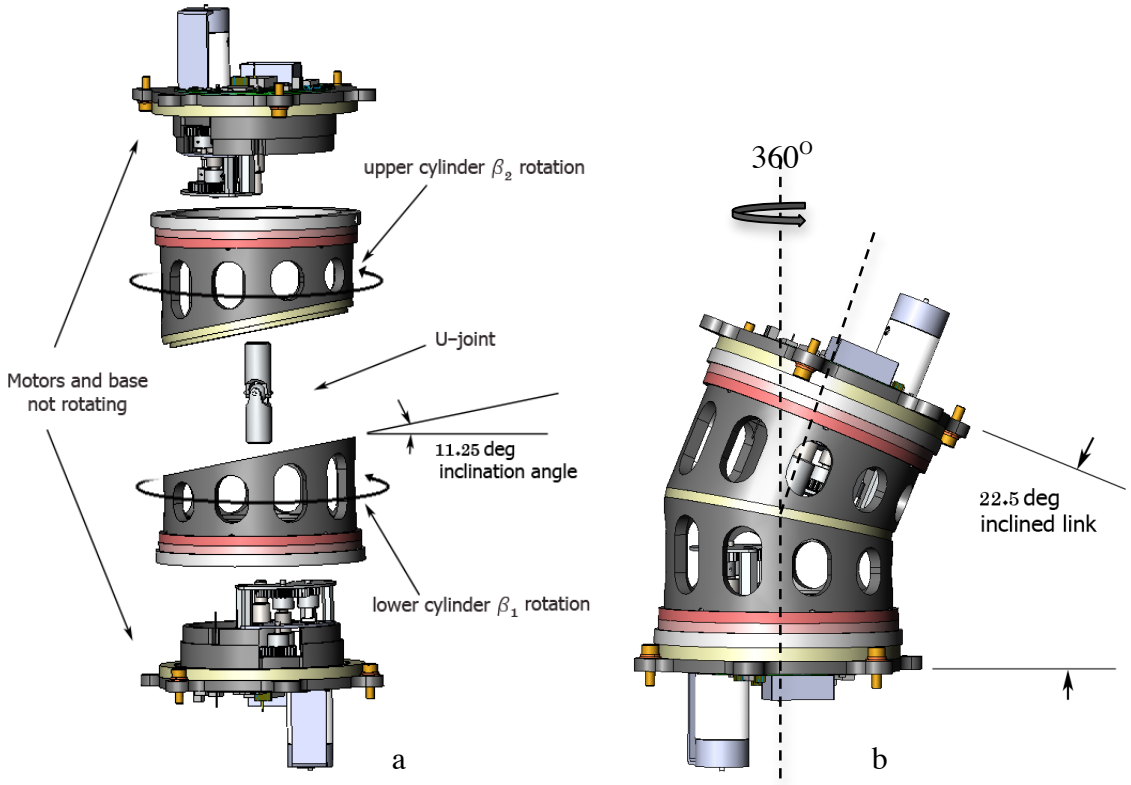

Figure 2: a) Exploded view of a link b) Link bent at 22.5°.

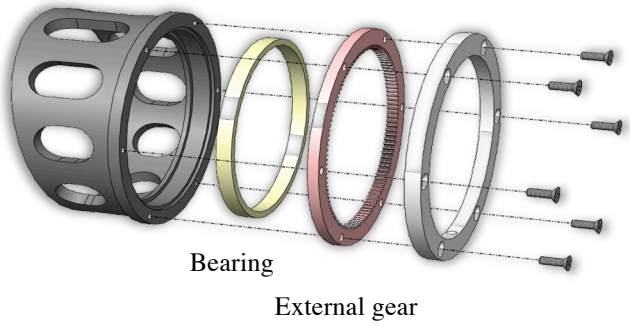

Figure 3: Cylinder components.

As can be observed in Figure 2a, inclination and orientation of the inclined link are achieved using rotational motors; both rotations occur only at the inclined cylinders, while the base of the link is not rotating, and acts as a support for the motor and gear. This kinematic

arrangement results in a backbone composed of passive universal joints, which is supported and actuated by the cylindrical structure that serves as an exoskeleton. Consequently, this mechanical design can withstand high bending and twisting torques because bending torques resulting from self-weight and external loads are handled by the exoskeleton structure, i.e. at the inclined plane connecting the two cylinders and the contact planes with the link bases. Furthermore, the torque applied on the motors results only from the friction forces along the inclined plane or the base planes when the inclination or orientation changes. Relative to the HRR arm self-weight, these torques are very low and can be further reduced by lowering the friction coefficient between the surfaces.

For actuation, we used 4W Maxon RE-Max17 DC motors with an internal 128:1 gear ratio and 128 CPT encoders. The motor axis is connected to an external gear (Figures 3 and 4), having three stages with an overall ratio of 1:22. PTFE Journal bearings were used against the 7075-T6 aluminium base and cylinders to achieve light weight and low friction.

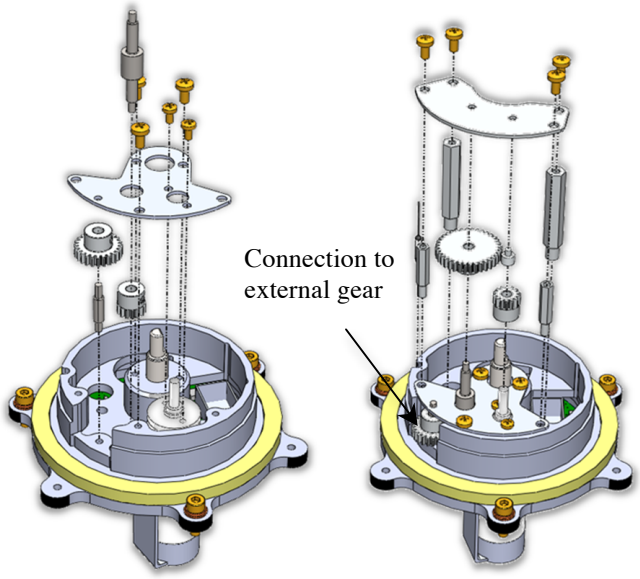

Figure 4: Base of a link and gear assembly.

2.2 Low level controller

Distributed control architecture was implemented by having a local control board connected to a groove at the back of the base of each link (Figure 5). A RS485 communication central

data bus connects all the local control boards to a single high-level controller where motion planning and inverse kinematics are performed.

Each control board, located between two link bases, consists of a DSP MCU (dsPIC33FJ128MC204), an integrated 3A H-Bridge driver, a Quadrature Encoder interface including differential line decoders and supports two adjacent DC motors and encoders.

Each control board is connected to a central power bus (14AWG main electric dual cable) delivering 24V. As mentioned in the previous section, an important mechanical feature of the mechanism is that the bases of the link are fixed and not rotating. This feature is important for keeping the electrical wires running along the mechanism from twisting, hence not limiting the rotation of all the links.

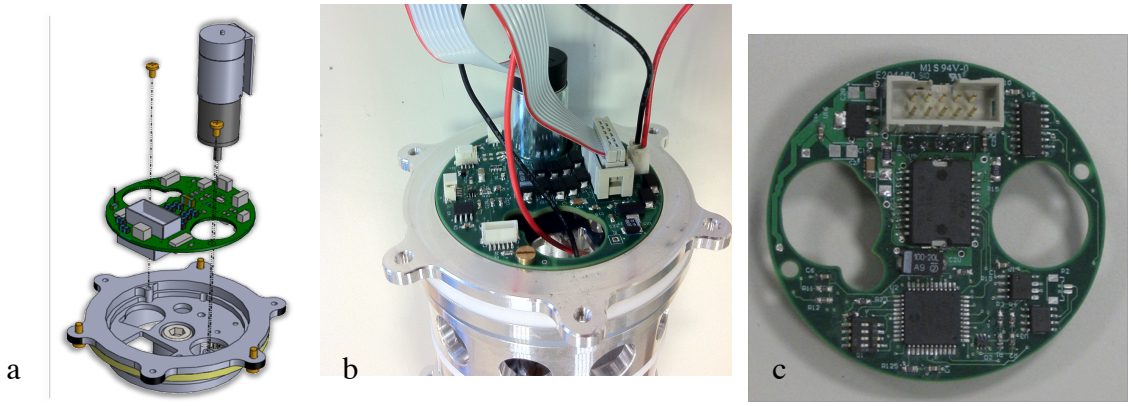

Figure 5: a) Controller assembly in a groove at the back of the base b) physical model c) PWB layout.

Position control feedback is achieved using the DC motor encoders, with an additional magnetic reed switch used as the index for each half link full rotation which enables homing of each link (Figure 6). The reed switch is located inside a through hole in the base which does not rotate, while a magnet is located inside the rotating cylinder connected to the outer gear as seen in Figure 6.

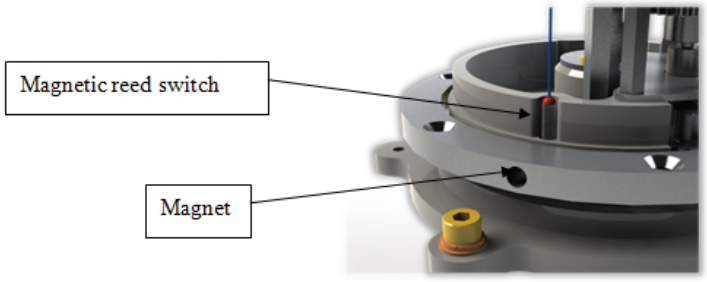

Figure 6: Magnetic index.

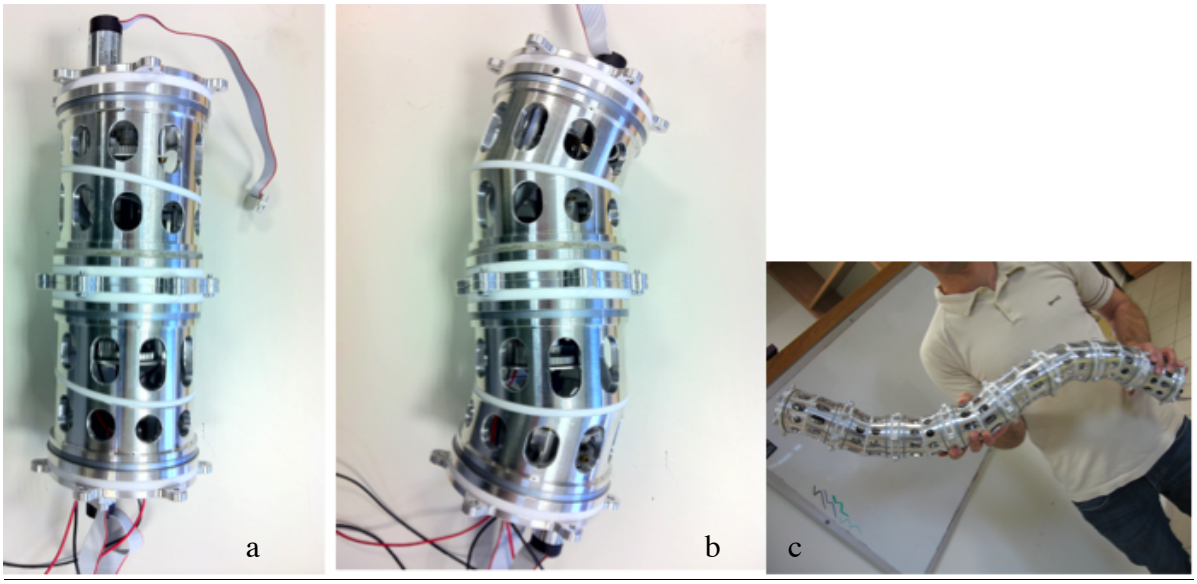

Figure 7: Working model; a) two non-inclined links b) two inclined links c) full assembled arm.

2.3 Motor torque calculation

The maximal applied torque on each motor can be calculated at a fully stretched configuration (Figure).

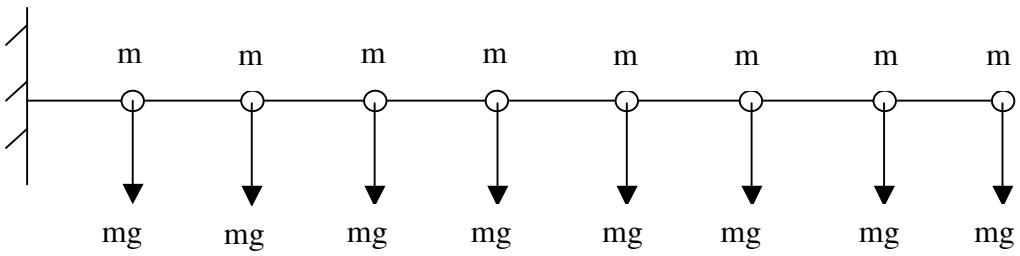

Figure 8: Static self load of the mechanism for maximal torque calculation.

The bending torque in each link is given by:

$$M_{Bi} = \sum_{j=1}^{i} m_j g l_{i-j} \quad (1)$$

Starting from the payload link (1) to the current link (j)

The axial force in each link can be written as a function of the bending torque and is given by:

$$F_i = \frac{M_{Bi}}{r} \quad (2)$$

Hence, the torque applied on each motor is given by:

$$T_i = \frac{F_i \cdot \mu \cdot r}{\eta \cdot G} \quad (3)$$

Where:

l_{i-j} - Distance from link i to current link j

r - Effective link radius

μ - Friction coefficient

G - Gear ratio

η - Gear efficiency

A modular identical design for all links was chosen, which will simplify the design and lower overall costs. Hence, for the calculation of the required motor's torque, we refer to the base motor, which bears the maximal torque.

$$T_n = \frac{\mu \cdot M_{Bn}}{\eta \cdot G} \quad (4)$$

The linear dependency between the motor torque required and the friction coefficient for each of the links along the arm can be observed in Figure , where each line refers to a different link and the fixed link requires the highest torque. The friction coefficient of PTFE and aluminium is about 0.15, which is indicated in Figure . It is worth mentioning that the friction coefficient can be reduced even further by thrust bearings or better yet by using special low-friction coatings on the aluminium which have no additional weight and which are known to reduce the friction coefficient to as low as 0.02 [17]; consequently; the base motor torque can be reduced from 180 mN to 25 mN, meaning smaller and lighter motors or an improved capability to lift heavier payloads.

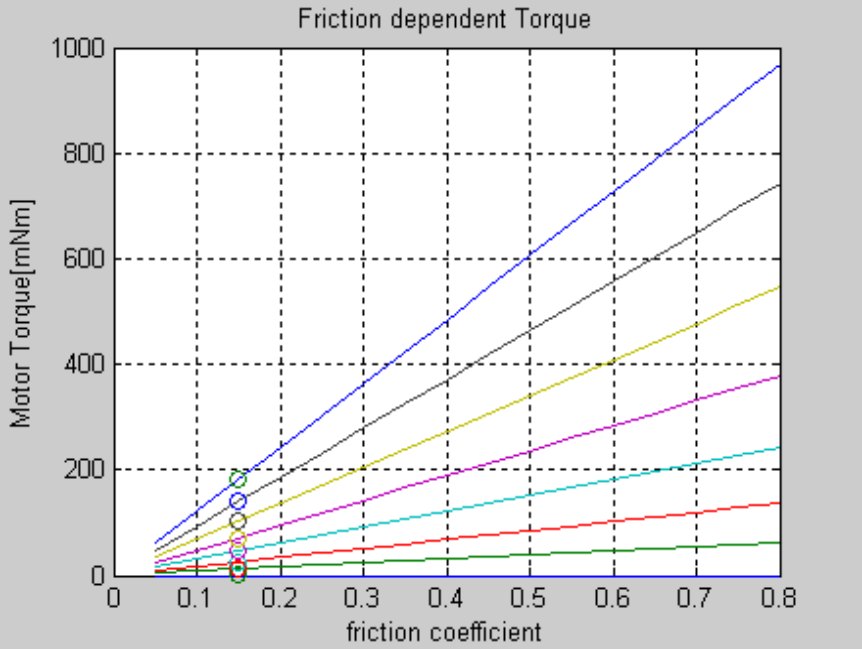

Figure 9: Motor torque is friction dependent.

3. Forward kinematics of the mechanism

The backbone of the mechanism is basically a series of universal joints, which are never twisted around their axis but only bent using rotational actuators. Hence, the kinematics of each link can be modelled as two revolute joints perpendicular to each other and to the trunk's backbone axis (Figure 10). Moreover, the actual angle of rotation of the motor is a function of the bending angle of the universal joint. The forward kinematics solution of the arm is given using the Denavit-Hartenberg convention, accordingly (Table 1).

The resulting transformation matrix that expresses the position and orientation of the origin of the end effector with respect to the base frame is given by a multiplication of all the local transformation matrices between two successive joints:

$$A_{16}^{0} = A_{1}^{0} A_{2}^{1} \cdots A_{16}^{15} \tag{5}$$

Where, for example:

$$A_{1}^{0} = \begin{bmatrix} \cos(\theta_1) & -\sin(\theta_1)\cos(\alpha_1) & \sin(\theta_1)\sin(\alpha_1) & a_1\cos(\theta_1) \\ \sin(\theta_1) & \cos(\theta_1)\cos(\alpha_1) & -\cos(\theta_1)\sin(\alpha_1) & a_1\sin(\theta_1) \\ 0 & \sin(\alpha_1) & \cos(\alpha_1) & d_1 \\ 0 & 0 & 0 & 1 \end{bmatrix} = \begin{bmatrix} \cos(\theta_1) & 0 & \sin(\theta_1) & 0 \\ \sin(\theta_1) & 0 & -\cos(\theta_1) & 0 \\ 0 & 1 & 0 & 0 \\ 0 & 0 & 0 & 1 \end{bmatrix}$$

$$A_2^1 = \begin{bmatrix} \cos(\theta_2) & -\sin(\theta_2)\cos(\alpha_2) & \sin(\theta_2)\sin(\alpha_2) & a_2\cos(\theta_2) \\ \sin(\theta_2) & \cos(\theta_2)\cos(\alpha_2) & -\cos(\theta_2)\sin(\alpha_2) & a_2\sin(\theta_2) \\ 0 & \sin(\alpha_2) & \cos(\alpha_2) & d_2 \\ 0 & 0 & 0 & 1 \end{bmatrix} = \begin{bmatrix} \cos(\theta_2) & 0 & -\sin(\theta_2) & 98\cos(\theta_2) \\ \sin(\theta_2) & 0 & \cos(\theta_2) & 98\sin(\theta_2) \\ 0 & -1 & 0 & 0 \\ 0 & 0 & 0 & 1 \end{bmatrix}$$

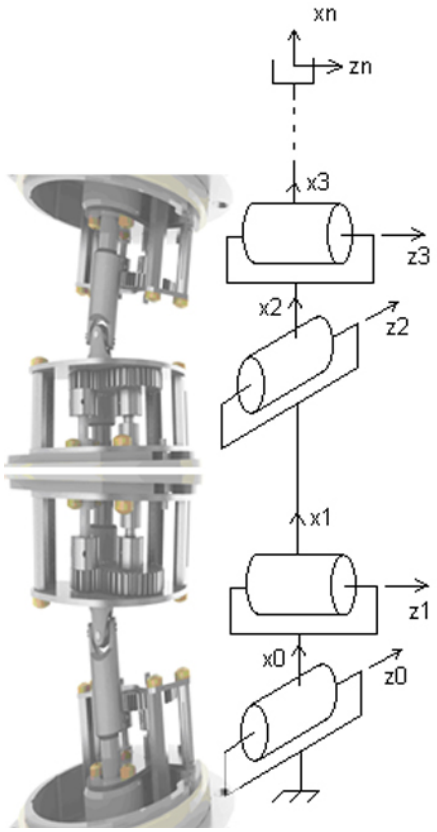

Figure 10: Kinematics scheme.

n	θ_i	d_i	a_i	α_i
1	θ_1	0	0	90
2	θ_2	0	98	-90
3	θ_3	0	0	90
4	θ_4	0	98	-90
5	θ_5	0	0	90
6	θ_6	0	98	-90
7	θ_7	0	0	90
8	θ_8	0	98	-90
9	θ_9	0	0	90
10	θ_{10}	0	98	-90
11	θ_{11}	0	0	90
12	θ_{12}	0	98	-90
13	θ_{13}	0	0	90
14	θ_{14}	0	98	-90
15	θ_{15}	0	0	90
16	θ_{16}	0	98	-90

Table 1: DH convention.

As mentioned, θ_i and θ_{i+1} are the two bending angles of each U-joint. Both angles are a function of the rotation angles β_i and β_{i+1} of both inclined cylinders in each link (Figure 2). The β_i and β_{i+1} angles are the rotation angles of the motors multiplied by the overall gear ratio, N=22:

θ_i and θ_{i+1} are given by:

$$\theta_i = \alpha(\cos(\beta_i) - \cos(\beta_{i+1})) \quad (6)$$

$$\theta_{i+1} = \alpha(\sin(\beta_i) - \sin(\beta_{i+1})) \quad (7)$$

Where:

α - Inclination angle of the rotating inclined cylinders ($\alpha = 11.25^{o}$)

β_i - Rotation angle of the lower inclined cylinder

β_{i+1}- Rotation angle of the upper inclined cylinder

The bending angles of the universal joints for both of its perpendicular revolute joints can be extracted from equations 6 and 7. These angles are plotted in Figure for a fixed lower cylinder angle i.e. β_1=0, while the upper cylinder, i.e. β_2, goes through a full rotation.

As can be observed, in this case, the upper cylinder bends to a full inclination of θ_1=22.5° at β_2 - β_1=180°, and half of the maximum inclination, of both θ_1 and θ_2= ±11.25° at β_2 - β_1 =90° and 270°.

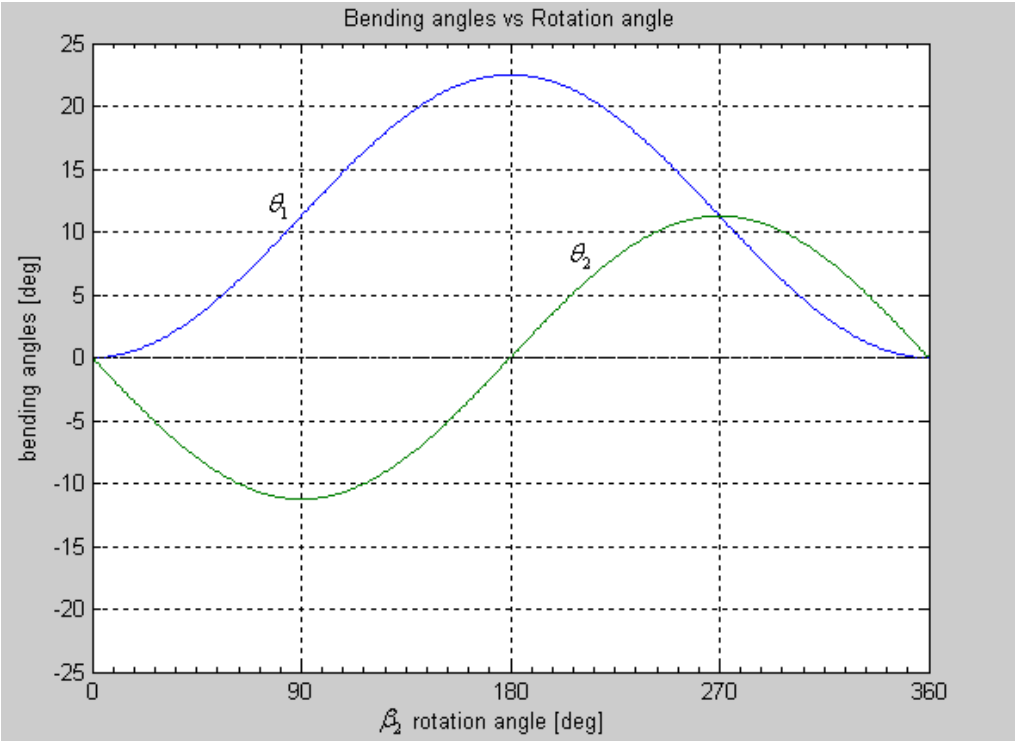

Figure 11: Bending angles vs. rotation angle.

4. Inverse kinematics of link

The inclined cylinder design and the way they are actuated define a kinematics dependency between the orientation of the inclination plane and the magnitude of inclination (angle) of the upper cylinder relative to the lower one.

Figure 12 shows a top view of a link, which can be regarded as a polar arrow, where the orientation of the arrow refers to the orientation of the inclination plane of the link (between 0-360°), while the length of the arrow refers to the magnitude of the inclination angle (between 0-22.5°).

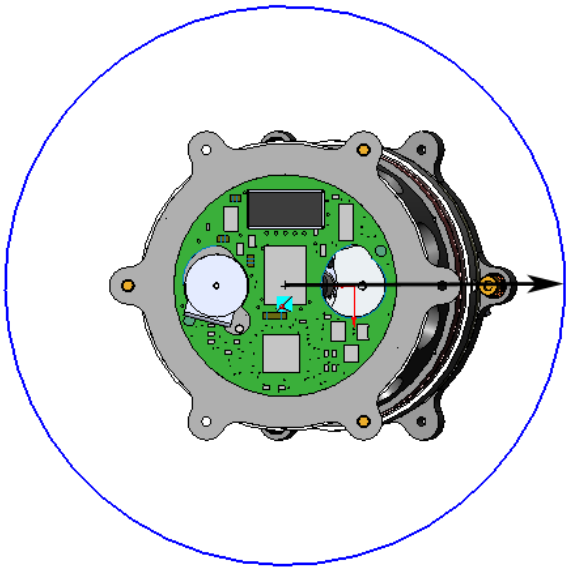

Figure 12: Direction and magnitude of inclination.

The inverse kinematics solution, as a means for path planning of the full length of the arm, should define these two different motions independently, as a function of each cylinder (or motor) rotation β_i and β_{i+1}.

In order to choose the orientation of the inclination plane, one must rotate both β_1 and β_2 at the same speed, meaning keeping $\beta_2 - \beta_1$=constant, where this constant is a measure of the magnitude of inclination. In Figure 13, we set $\beta_2 = \beta_1 + 180$, meaning an initial full inclination

of 22.5° and rotation of both cylinders in the same direction a full revolution of 360°. As can be seen, θ_2 follows θ_1 by 90°, reaching the same amplitude (magnitude of inclination angle).

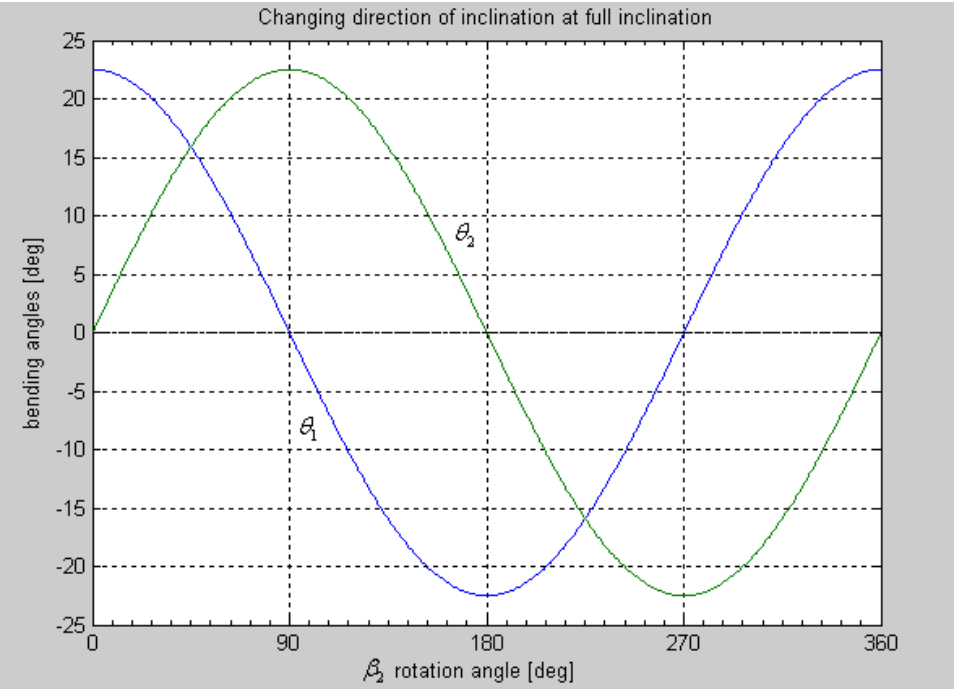

Figure 12: Changing the direction of inclination at full inclination $\beta_2 = \beta_1 + 180$.

In order to keep the orientation of the inclination plane constant while changing the magnitude of inclination, one must rotate both β_1 and β_2 at the same speed but in opposite directions, meaning $\beta_2 + \beta_1 =$constant, where this constant now determines the direction of inclination. In Figure 14, we set $\beta_1 = 0$ and kept $\beta_2 = \beta_1$ during rotation, and as can be seen in Figure 14, $\theta_1 = 0$ while θ_2 is changing and reaching an amplitude of 22.5° in both directions (magnitude of inclination).

The set of kinematics transformations presented are the inverse kinematics solution of a link. This means that once a set of θ angles are determined using an inverse kinematics solution for the entire arm, the local β_1 and β_2 angles for each link can be determined resulting in motor commands if the overall gear ratio is known.

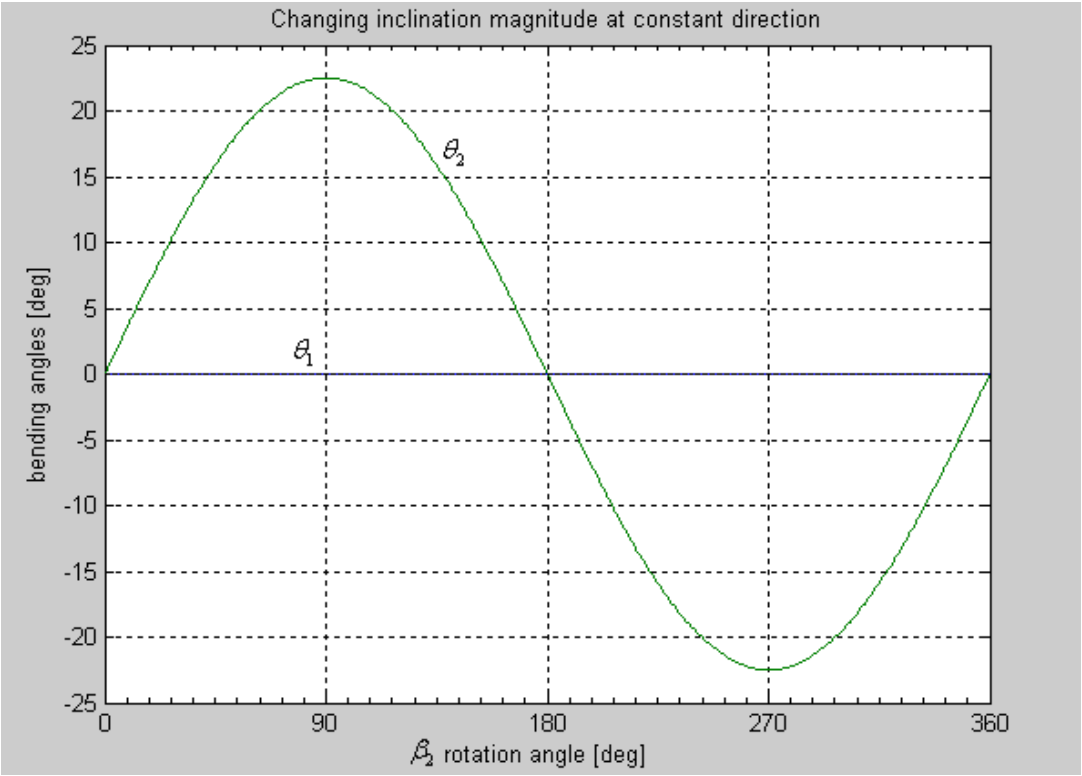

Figure 13: Changing inclination magnitude in a constant direction $\beta_2 + \beta_1 = 0$.

4. Conclusions

In this report, we describe the mechanical structure and kinematics analysis of a novel hyper-redundant robotic arm. The arm is composed of sixteen rotational degrees of freedom and is design to achieve high rigidity and accuracy. The arm is composed of two concentric skeletons: internal and external. The internal skeleton is responsible for the kinematics of the arm and serves as a backbone, whereas the external skeleton serves as a mechanical "exoskeleton" carrying the self-weight of the arm and the external loads.

We use distributed low-level controllers to control the arm. Connected to a RS485 data bus and a 24V power bus, each link runs its own PID control loop based on gait commands received over the data bus.

The forward kinematics of the mechanism are not straightforward, that is, the bending angles of the arm are not directly related to motor angle. We therefore derived the inverse kinematics transformation for a link by deriving the kinematic linkage between the arm tilt angles and motor angles.

There are many daily applications where such an arm may be useful. For example, this type of hyper-redundant arm can be very useful for search and rescue applications when it is mounted on a mobile platform with a camera mounted on its end-effector, to be used to look for survivors trapped inside collapsed rubble. This use will lower the risk of rescue workers finding themselves trapped due to secondary collapse of structures [14]. Another application for such an arm is remote bomb disposal. The arm allows for a large workspace combined with delicate and stable manoeuvres via its gripper, unlike some of the current robots which have an arm moving in a vertical plane. Currently, with these platforms, the operator is obliged to manipulate the mobile platform in order to reach out of plane.

References

[1] S. Hirose, *Biologically Inspired Robots: Snake-like Locomotors and Manipulators*: Oxford University Press, 1993.

[2] G. S. Chirikjian and J. W. Burdick, A modal approach to hyper-redundant manipulator kinematics, *IEEE Transactions on Robotics and Automation"*, vol. 10, pp. 343-354, 1994.

[3] W. M. Kier and K. K. Smith, Tongues, tentacles, and trunk: the biomechanics of movement in muscular hydrostats, *Zoological Journal of the Linnean Society*, vol. 8, pp. 307-324, 1985.

[4] M. A. Hannan and I. D. Walker, "A Novel 'Elephant's Trunk' Robot", presented at 1999 IEEE/ASME International Conference on Advanced Intelligent Mechatronics, Atlanta, Georgia, 1999.

[5] Yim http://robotics.stanford.edu/users/mark/bio.html; last accessed 06/2011.

[6] G. Miller, *Snake robots for research and rescue*. Cambridge, MA: The MIT Press, 2002.

[7] "G. Miller http://www.doctorgavin.com/ last accessed 06/2003."

[8] G. L. Haith, H. Thomas, and A. Wright, "A Serpentine Robot for Planetary and Asteroid Surface Exploration", presented as an oral presentation at the Fourth IAA International Conference on Low-Cost Planetary Missions, Laurel, MD, 2000.

[9] H. Ikeda and N. Takanashi, "Joint Assembly Movable Like a Human Arm", vol. 4,683,406, U.S. Patent, 1987.

[10] N. Takanashi, K. Aoki, and S. Yashima, "A Gait Control for the Hyper-redundant Robot O-RO-CHI", presented at Proc. of ROBOMEC '96, Ube, Japan, 1996.

[11] JPL http://technology.jpl.nasa.gov/gallery/techGallery/gallery/gl_pages/P44487.html; accessed 6/2011.

[12] R. Cieslak and A. Morecki, Elephant trunk type elastic manipulator - A tool for bulk and liquid materials transportation, *Robotica*, vol. 17, pp. 11-16, 1999.

[13] S. Ma, H. Hirose, and H. Yoshinada, Development of a hyper-redundant multijoint manipulator for maintenance of nuclear reactors, *International Journal of Advanced Robotics*, vol. 9, pp. 281-300, 1995.

[14] A. Wolf, H. Choset, H. B. Brown, and R. Casciola, Design and control of a mobile hyper-redundant urban search and rescue robot, *International Journal of Advanced Robotics*, vol. 19, pp. 221-248, 2005.

[15] V.A. Sujan, S. Dubowsky, Design of a lightweight hyper-redundant deployable binary manipulator", ASME Journal of Mechanical Design, vol. 126, pp 29-39, 2004.

[16] S. Hirose, T. Ishii, A. Haishi, Float arm V: hyper redundant manipulator with wire-driven weight-compensation mechanism, Proceedings ICRA, pp. 368-373, 2003.

[17] Erdemir, A. and Fenske, G. R., Clean and cost-effective dry boundary lubricants for aluminum forming, SAE Publ. No. SP-1350, pp 9-17, 1998.